Boosting the Magnetic Field of a Torus-shaped Conductive Fluid via Poloidal Flow

Mamoru Otsuki[1*]

[1*]Independent, Tokyo, Japan.

Corresponding author(s). E-mail(s): gangankeisun@nifty.com;

Abstract

Researchers have struggled to understand the mechanism underlying the formation of celestial magnetic fields. Currently, the generation of axisymmetric and poloidal magnetic fields can be solved by complex convection arguments. There are also claims of simple convection, but these claims are not purely simple axisymmetric convection claims. This paper addresses a truly simple axisymmetric poloidal convection and magnetic field. To calculate the electrical components, this paper introduces a theory that separates the vector potential into inductance and current in a relational formula. The reason is to consider the mutual influence between distant circuits in terms of mutual inductance. The change in current is subsequently calculated from the change in inductance. It is solved as an eigenvalue problem via numerical calculation. Using this method, a simple axisymmetric poloidal magnetic field can be generated from axisymmetric poloidal convection. Another reason is the nature of the mutual inductance and Lenz's law, which reflects the effect of current changes on other electric circuits. This approach is intended to eliminate the concern that magnetic field growth will be impaired by convection that carries currents away. These concepts are novel, and we believe that these findings will contribute to further elucidating the formation mechanism of celestial magnetic fields and plasma reactor research. However, some issues in this paper remain unresolved.

Keywords: poloidal flow, dynamo theory, inductance, numerically calculated eigenvalues, magnetohydrodynamics

1 Introduction

1.1 Magnetic Field Study of Celestial Bodies

Researchers have long struggled to understand the mechanism underlying the formation of celestial magnetic fields. Research in this field could progress through the discovery of a new underlying mechanism. Currently, the generation of axisymmetric and poloidal magnetic fields can be solved by complex convection arguments.

For example, the famous foundations for elucidating the mechanism of the formation of celestial magnetic fields are the ω effect[1], the α effect[2], and Cowling's theorem[3].

Taking the Sun as an example, the magnetic field in the plane perpendicular to the axis of rotation of the Sun is called the toroidal magnetic field, and the magnetic field in the plane parallel to the axis of rotation is called the poloidal magnetic field. The same is true for convection. According to Cowling's theorem, axisymmetric convection does not generate a stable axisymmetric magnetic field, either poloidal or toroidal.

The ω effect generates a toroidal magnetic field from a poloidal magnetic field where a gradient in angular velocity exists. Since the rotation of the surface of the Sun is faster at the equator than at the poles, an angular velocity gradient exists. If the initial magnetic field is poloidal, the magnetic field is stretched such that the angular velocity gradient winds it up, and the poloidal magnetic field becomes toroidal. If the toroidal magnetic field is changed to a poloidal magnetic field, the magnetic field may be amplified. However, no such effect was found. In the end, the result was in favour of Cowling's theorem.

The α effect assumes a velocity field that twists a magnetic field. The concept is to twist the toroidal magnetic field in some places and direct it in the poloidal direction. Therefore, if an α effect is added to the ω effect, mutual exchange of magnetic fields is possible, and the magnetic field may be amplified. However, this approach is not as easy to use as described above. Researchers have combined these effects with complex convection to further elucidate the mechanism of magnetic field generation[4][5]. To our knowledge, few papers[6][7][8] have argued for the generation of magnetic fields by simple convection. However, these claims are not purely simple axisymmetric convection claims.

The notion that a magnetic field is generated by complex convection or that an axisymmetric magnetic field does not occur constrains the study. A discussion of the generation of magnetic fields by complex convection is meaningful and necessary. However, in the observations, the difference between the axis of rotation and the magnetic axis is not large for the main celestial bodies in the solar system[1], especially for Saturn[9]. A theory that convection and magnetic fields are simply axisymmetric could facilitate a discussion.

Clarifying that simpler convection can generate a magnetic field will further advance research in this field. This paper[2] explores the possibility of generating a magnetic field by convection, which is simpler.

[1] Note that this statement was made as a motivation for this study, and it is not known whether the results of this study are reflected in the nature of these celestial magnetic fields

[2] An earlier version of our original manuscript is available on a preprint server[10].

In this paper, we suggest the generation of a purely simple axisymmetric magnetic field via the following method.

1.2 Methods for this Research

The plurality of circuits (coils) and inductances described in this paper are briefly shown in the figure below. The inductance is important for understanding this phenomenon. Here, an overview of how inductance is handled is provided. Poloidal convection is considered axisymmetric (Fig. 1). This figure shows convection, in which a torus-shaped (doughnut-shaped) fluid moves in the direction indicated by $\boldsymbol{U}$. Since it is a convection of a conductive fluid, it is thought that multiple coaxially toroidal circular electrical circuits (hereinafter referred to as coils) move as bundles in a poloidal manner. The abovementioned inductance is the inductance of these coils. This term refers to the self-inductance and the mutual inductance between the coils. There are an infinite number of these coils, but in the numerical calculations described below, 16 circuits are set to move in the direction indicated by $\boldsymbol{U}$ on the torus surface, as shown in the cross-sectional view of the circuit (Fig. 2). The convection and coil settings are described in detail in Section 2.1, Description of the Problem.

First, a formula is needed. We derive the basic electromagnetic induction equation to determine whether power generation starts and lasts. The relevant electromagnetic induction equations are expressed by the vector potential[11]. Furthermore, this vector potential is converted into an expression of inductance[11]. This conversion separates the vector potential into an inductance component representing the structure of the fluid and an electrical component representing the current.

The reason is to consider the mutual influence between distant circuits in terms of mutual inductance. The change in current is subsequently calculated from the change in inductance. We believe that the difference in the movement of convection between the position where power generation is highest and the position of the surrounding position causes power generation. Here, the position refers to the position on the plane parallel to the axis of rotation (the Z-Y or Z-Ra plane described later). Therefore, power generation is not generated by convection at a single position but by the behaviour of the surrounding convection. This problem must be solved not only at one place where power generation is at the top but also by integrating the self- and mutual inductance of multiple coils.

Another reason is to consider mutual inductance in combination with Lenz's law[12]. This combination eliminates the concern that magnetic field growth is impaired by convection, which carries away coils with currents. This idea is discussed in detail in Section 4.4, The Problem of Coils with Currents being Carried Away by Convection.

This electromagnetic induction equation is set and combined in a plurality of circuits. This problem is solved via numerical calculation as an eigenvalue problem. As a solution, the eigenvalues and eigenvectors are obtained. These results imply a change in the current and current distribution in the circuits. The results are shown in the tables and figures, showing the possibility of generating magnetic fields and the distribution of axisymmetric magnetic fields. Thus, it is shown that an axisymmetric

magnetic field can be generated from axisymmetric convection without particularly complex convection.

1.3 The Role of the Formulas

A coil moving in a poloidal manner with convection moves in the radial direction and the cylindrical axial direction of the cylindrical coordinates. In this way, the coil moves in the existing magnetic field, and power generation occurs. The derived equation shows the relationship between this convection and power generation. However, a magnetic field is not always present. A magnetic field in the appropriate direction must also be generated by power generation. This process is called self-excitation power generation. We would like to suggest that electricity can be generated by integrating the entire torus. For this purpose, the equation is applied to a plurality of coils at different positions and solved as an eigenvalue problem. If power generation is recognised as a result of the calculation, the possibility of overall self-excited power generation of the torus can be explained.

Thus, the eigenvalues and eigenvectors are obtained from the numerical calculations. The eigenvalue of the positive polarity indicates the growth of the eigenvector (the current distribution of the coil), which suggests the growth of the magnetic field. Furthermore, the magnetic field distribution obtained from the eigenvector components calculated as the current flows through each coil is also shown in the figure. On the basis of these results, the possibility of self-excited power generation that creates an axisymmetric poloidal magnetic field is explained.

1.4 Stable Magnetic Field

Here, the possibility of growth of the magnetic field is shown, but the stability of the magnetic field is not indicated. We believe that a stable magnetic field is possible in relation to convection. This possibility is shown in Section 4.2, Possibility of Magnetic Field Stabilisation. However, since convection behaviour is not the subject of this paper, we discuss only the possibility of maintaining the stability of the magnetic field. Even if this stability is insufficient, we believe that these results and ideas will be useful for future research. We also believe that this argument can be applied to more than celestial bodies. This possibility is shown in Section 5, Conclusion.

1.5 Unresolved Issues

Some issues in this paper remain unresolved, such as a stable magnetic field and magnetic diffusivity. These issues are discussed in Section 4, Discussion.

2 Mechanism

2.1 Description of the Problem

In this paper, we solve and discuss axisymmetric convection and magnetic fields via numerical calculations. Here, the geometric structure of convection and the knowledge necessary to calculate coil inductances are explained via figures.

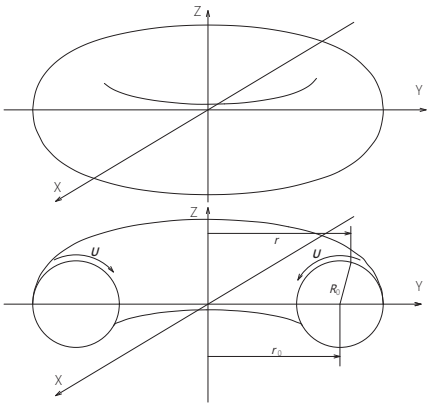

Fig. 1 Schematic of the toroidal geometry. This schematic is an approximate geometric outline of convection set by numerical calculations. A torus-like conductive fluid flows in a poloidal direction U. The upper figure is the whole, and the bottom figure is the cross section.

To determine whether a magnetic field can fluctuate in the poloidal stream of a conductive fluid, a certain poloidal flow is set, and the induction equation (as a simultaneous equation expressed by inductances) is expressed in terms of toroidal vector potentials to calculate the current as an eigenvalue problem. The poloidal flow of a fluid occurs in a torus shape (Fig. 1). The upper figure is the whole, and the bottom figure is the cross section, where $\boldsymbol{U}$ is the poloidal velocity, R_0 is the radius of the poloidal flow, and r is the radius of an example position on the torus from the Z axis. The number of coils in the coil bundle is infinite. Here, only a part of the coils shown below are considered.

A representative cross section (Z-Y plane) of the torus is shown (Fig. 2(a)). The stream is divided into toroidal segments for calculation as coils (Fig. 2(b)). That is, Fig. 2(a) and (b) show the right half of the cross section of Fig. 1. Z is the centre axis, and Ra is the radial axis of the cylindrical coordinates (equivalent to the Y axis in Fig. 1), where the circle indicates the cross section of the torus. P_c is the centre of the flow, where r_0 and z_0 are the elements of position P_c in the Ra and Z directions, respectively. Notably, P_0 is at the coordinates (0,0), and P_c is at (r_0,0). P is a representative position at which the flow velocity vector $\boldsymbol{U}$ is calculated; u_r and u_z are the elements of $\boldsymbol{U}$ in the Ra and Z directions, respectively; θ is the angle between the Ra axis and position P; and r is the element of position P in the Ra direction (Fig. 2(a)). Note that θ is not the zenith angle of the polar coordinates but the angle from the Ra axis. The coils used to define the flow torus are defined in Fig. 2(b). Sixteen coils are considered, where n refers to the number of coils. The dotted lines indicate the coaxial coils (i.e., the region occupied by the fluid), which are separated by the thickness T. Multiple coils wind only once around the Z axis, and the coils move in the direction of $\boldsymbol{U}$ with radius R_0. Therefore, the circumference of each coil expands and contracts. The electric current runs separately in each coil in the ϕ direction, which orbits the Z axis. Although the coils can move, the later calculation of the eigenvalues assumes that they are motionless in a brief moment Δt.

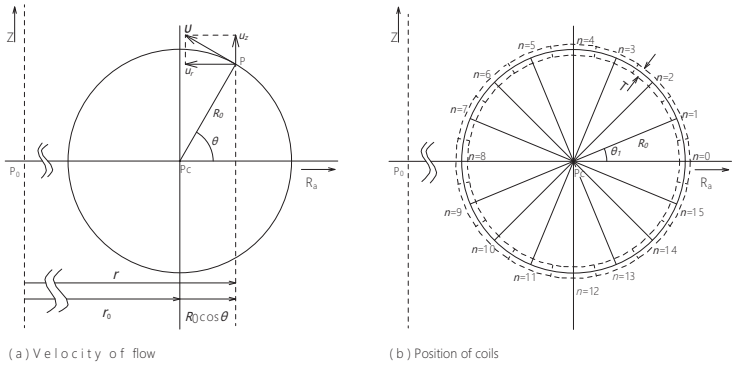

Fig. 2 Schematics of the (a) velocity of the fluid flow and (b) defined coils in the cross section of the convection (Z-Y or Z-Ra plane). This figure is a cross section of Fig. 1 and shows settings such as the arrangement of the virtual coils used in the numerical calculations.

The top and side views of a set of any two coaxial coils are shown (Figs. 3(a) and (b)). These figures explain the relationship between the electric current $\boldsymbol{I}$ and vector potential[11] $\boldsymbol{A}$ for the calculation of inductances[11]. X, Y, and Z are the axes of the rectangular Cartesian coordinate system (Fig. 3). C_j is Coil j, in which the current $\boldsymbol{I}_j$ flows, and C_i is Coil i, which obtains the vector potential[11] $\boldsymbol{A}_j$ induced by the current $\boldsymbol{I}_j$ running in Coil C_j. ϕ is the angle of rotation around the Z axis, starting from the Y axis. Here, r_i and r_j are the radii of C_i and C_j, respectively. Furthermore, ds_i and ds_j are infinitesimal lengths of C_i and C_j , respectively, on each coil for integration, where ds_i is placed on C_i ($\phi = 0$) and where ds_j is placed on $\mathrm{P}_{j\phi}$ at ϕ with a distance l between them. $\boldsymbol{I}ds_j$ is the contribution to the current over ds_j, where $\boldsymbol{A}ds_j$ is the vector potential induced on ds_i by $\boldsymbol{I}ds_j$. $\boldsymbol{A}_j$ is the element of $\boldsymbol{A}ds_j$ in the X direction. Φ_i is the total flux linked in C_i. The side view is also a schematic version of Fig. 2. The symbols are the same as those in Fig. 2. The dashed circle approximately indicates the convection of the fluid. P_j and P_i are the positions of the two coils in the Z-Ra plane.

In addition, a 3D image of the coils is shown to clarify their relationships with each other (Fig. 4). Each coil is arrayed coaxially with the Z axis, and the coils are parallel to each other.

2.2 Calculation of the magnetic properties

In the numerical calculations in this paper, the electromagnetic induction equations are applied to multiple coils, and the current is calculated by combining these equations to solve them as an eigenvalue problem. Here, the underlying electromagnetic induction equation is derived. In addition, a method for calculating the inductance to be included in the numerical calculation is described.

2.2.1 Derivation of Basic Formulas

As a source equation for determining the relationship between the electric current and magnetic field, Ohm's law[11] is used with an electric field to calculate the current as follows:

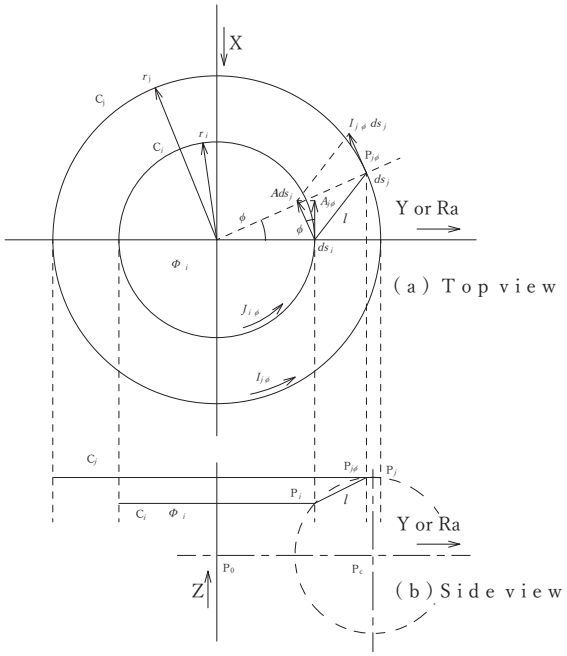

Fig. 3 Relationship between the electric current $\boldsymbol{I}$ and vector potential $\boldsymbol{A}$ for the set of coils shown in Fig. 2: (a) top view and (b) side view of the coils on the torus. Two virtual coils are used to explain how to calculate self- and mutual inductance.

$$\boldsymbol{J} = \sigma\left(\boldsymbol{E} + \boldsymbol{u} \times \boldsymbol{B}\right) \tag{1}$$

Here, $\boldsymbol{J}$ is the current density; σ is the electrical conductivity; $\boldsymbol{u}$ is the velocity of the conductive fluid; $\boldsymbol{B}$ is the magnetic field, which can be found via (2); $\boldsymbol{u} \times \boldsymbol{B}$ is the motion of the electric field; and $\boldsymbol{E}$ is the electric field potential, which can be found via (3)[11] as follows:

$$\boldsymbol{B} = \nabla \times \boldsymbol{A} \tag{2}$$

$$\boldsymbol{E} = -\frac{\partial \boldsymbol{A}}{\partial t} + \nabla\varphi \tag{3}$$

Here, φ is a scalar potential, $\boldsymbol{A}$ is a vector potential[11], and t represents the time.

To derive an induction equation expressed in vector potentials from Ohm's law (1), these equations are combined as follows:

$$\frac{\partial \boldsymbol{A}}{\partial t} - \boldsymbol{u} \times (\nabla \times \boldsymbol{A}) = \nabla\varphi - \frac{\boldsymbol{J}}{\sigma} \tag{4}$$

To apply this induction equation for coils, the factor $2\pi r_i$ (r_i=coil C_i radius) is multiplied as an integral around the coil on both sides of the equation because $\boldsymbol{A}$ and the current density are the same around C_i.

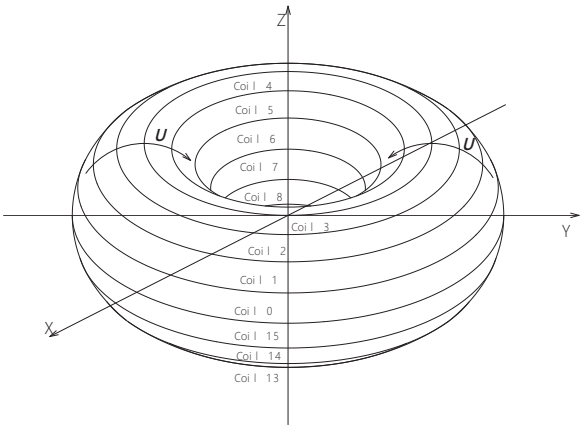

Fig. 4 3D view of the coaxial coils. A bird's-eye view is used to facilitate imagining the arrangement of the virtual coil.

$$\frac{\partial}{\partial t}\left(2\pi r_i \boldsymbol{A}\right) - \boldsymbol{u} \times \left(\nabla \times 2\pi r_i \boldsymbol{A}\right) = -\frac{2\pi r_i}{\sigma}\boldsymbol{J} \tag{5}$$

Here, φ is ignored because it is assumed that going around along C_i at that gradient will result in a value of zero. Furthermore, (6) shows the relationship between $\boldsymbol{A}$ and the inductance[11] (L). Here, the total magnetic flux linking the coil, Φ, is used in place of L, where $\Phi = LI$. The subscripts i and j refer to the coil numbers defined in Fig. 2, enabling the development of simultaneous equations.

$$\Phi_i = \oint_{C_i} \boldsymbol{A}_j ds_i \tag{6}$$

Here, Φ_i is the flux of coil C_i, and ds_i is an infinitesimal part of coil C_i. In this arrangement of coils, all the coils are arrayed coaxially with the Z axis and parallel to each other. Thus, $\boldsymbol{A}_j$ is the same around C_i. Therefore, $\Phi_i = 2\pi r_i \boldsymbol{A}_j$. When $\Phi_i = L_{ij} I_j$, the relationship between L_{ij} and $\boldsymbol{A}_j$ is as follows. L_{ij} is a matrix representing inductance, but only the diagonal element is self-inductance, and the other elements are mutual inductances, so it is hereafter referred to as M_{ij}.

$$\boldsymbol{A}_j = \frac{\boldsymbol{I}_j}{2\pi r_i} M_{ij}, A_{j\phi} = \frac{I_{j\phi}}{2\pi r_i} M_{ij} \tag{7}$$

$\boldsymbol{A}_j$ and $\boldsymbol{I}_j$ have only a toroidal component (indicated by the subscript ϕ) along the coil. Using (7), the vector potential is separated into an inductance component that expresses the structure of the fluid (electric circuits) and an electrical component that expresses the current. The reason is to consider the mutual influence between distant circuits in terms of mutual inductance. The change in current is subsequently calculated from the change in inductance. By substituting (7) into (5), the following equation is obtained:

$$\frac{\partial}{\partial t}\left(M_{ij} I_{j\phi}\right) - \left[\boldsymbol{u} \times \left(\nabla \times 2\pi r_i \boldsymbol{A}_j\right)\right]_\phi = -\frac{2\pi r_i}{\sigma}\boldsymbol{J}_i = -\frac{2\pi r_i}{\sigma} J_{i\phi} \tag{8}$$

Here, σ is the conductance of the fluid, and r_i is the radius from the Z axis. The current density $\boldsymbol{J}_i$ of the attenuation term of (8) is also described as $J_{i\phi}$ since it has only a ϕ direction component. However, the second term on the left-hand side of (8) is complicated. Thus, it must be addressed separately. This term is considered by decomposing it as follows:

$$\begin{aligned}
\boldsymbol{u} \times (\nabla \times \boldsymbol{A}_j) &= \begin{bmatrix} u_{ir} \\ 0 \\ u_{iz} \end{bmatrix} \times \begin{bmatrix} \frac{1}{r_i}\left(-r_i \frac{\partial A_{j\phi}}{\partial z_i}\right) \\ 0 \\ \frac{1}{r_i}\left(\frac{\partial r_i A_{j\phi}}{\partial r_i}\right) \end{bmatrix} \\
&= \begin{bmatrix} u_{ir} \\ 0 \\ u_{iz} \end{bmatrix} \times \begin{bmatrix} -\frac{\partial A_{j\phi}}{\partial z_i} \\ 0 \\ \frac{1}{r_i} A_{j\phi} + \frac{\partial A_{j\phi}}{\partial r_i} \end{bmatrix} \\
&= \begin{bmatrix} 0 \\ -u_{iz} \frac{\partial A_{j\phi}}{\partial z_i} - u_{ir}\left(\frac{1}{r_i} A_{j\phi} + \frac{\partial A_{j\phi}}{\partial r_i}\right) \\ 0 \end{bmatrix}
\end{aligned} \tag{9}$$

Here, $\mathrm{rot}\boldsymbol{A}_j$ is decomposed into cylindrical coordinates, and the subscripts r, ϕ, and z indicate the component directions in cylindrical coordinates, namely, the radius from the Z axis, the angle around the Z axis, and the Z direction, respectively. Since the current only runs through the toroidal coil, only the toroidal $A_{j\phi}$ component remains with the vector potential. Furthermore, since it is uniform in the toroidal direction, the $\frac{\partial}{\partial \phi}$ component is zero, and the description is excluded. Therefore, $\boldsymbol{A}_j$ only has a component in the ϕ direction. Thus, the other components of $\boldsymbol{A}_j$ are omitted. (10) is obtained by multiplying (9) by $2\pi r_i$, substituting (7) and including only the ϕ component as follows:

$$\begin{aligned}
&2\pi r_i \left[-u_{iz} \frac{\partial A_{j\phi}}{\partial z_i} - u_{ir}\left(\frac{1}{r_i} A_{j\phi} + \frac{\partial A_{j\phi}}{\partial r_i}\right)\right] \\
&= -u_{iz} \frac{\partial M_{ij} I_{j\phi}}{\partial z_i} - u_{ir}\left(\frac{1}{r_i} M_{ij} I_{j\phi} + \frac{\partial M_{ij} I_{j\phi}}{\partial r_i}\right) \\
&= -u_{ir} \frac{\partial M_{ij} I_{j\phi}}{\partial r_i} - u_{iz} \frac{\partial M_{ij} I_{j\phi}}{\partial z_i} - u_{ir} \frac{1}{r_i} M_{ij} I_{j\phi}
\end{aligned} \tag{10}$$

These terms are replaced by the second term on the left-hand side of (8) to obtain (11) as follows:

$$\begin{aligned}
&\frac{\partial}{\partial t}\left(M_{ij} I_{j\phi}\right) - \left(-u_{ir} \frac{\partial M_{ij} I_{j\phi}}{\partial r_i} - u_{iz} \frac{\partial M_{ij} I_{j\phi}}{\partial z_i} - u_{ir} \frac{1}{r_i} M_{ij} I_{j\phi}\right) \\
&\qquad = -\frac{2\pi r_i}{\sigma} J_{i\phi} = -\frac{2\pi r_i}{\sigma S} I_{i\phi}.
\end{aligned} \tag{11}$$

The term in (10) containing the vector potential $A_{j\phi}$ indicates the electromotive force when returning to Ohm's law (1). The electromotive force is unaffected by the cross-sectional area of the electric circuit. Furthermore, the attenuation term, including the current density $J_{i\phi}$, indicates a voltage drop. This voltage drop is affected by

the cross-sectional area of the circuit. (11) compares the electromotive force and the voltage drop. The $A_{j\phi}$ of the electromotive force term is derived from (7) and is expressed by the current $I_{j\phi}$, which is unaffected by the cross-sectional area of the electric circuit. The current density $J_{i\phi}$ of the attenuation term is $\frac{I_{i\phi}}{S}$. It is arranged as follows:

$$\frac{\partial}{\partial t}\left(M_{ij}I_{j\phi}\right) + u_{ir}\frac{\partial M_{ij}I_{j\phi}}{\partial r_i} + u_{iz}\frac{\partial M_{ij}I_{j\phi}}{\partial z_i} + u_{ir}\frac{1}{r_i}M_{ij}I_{i\phi} = -\frac{2\pi r_i}{\sigma S}I_{i\phi} \tag{12}$$

Since the first three terms on the left-hand side of (12) are equivalent to a total differential, they can be replaced as follows:

$$\frac{d}{dt}\left(M_{ij}I_{j\phi}\right) + u_{ir}\frac{1}{r_i}M_{ij}I_{j\phi} = -\frac{2\pi r_i}{\sigma S}I_{i\phi}$$

This equation can be transformed and rearranged as follows:

$$\frac{dM_{ij}}{dt}I_{j\phi} + M_{ij}\frac{dI_{j\phi}}{dt} + u_{ir}\frac{1}{r_i}M_{ij}I_{j\phi} = -\frac{2\pi r_i}{\sigma S}I_{i\phi}$$

$$\frac{dI_{j\phi}}{dt} = M_{ij}^{-1}\left(-\frac{dM_{ij}}{dt}I_{j\phi} - u_{ir}\frac{1}{r_i}M_{ij}I_{j\phi} - \frac{2\pi r_i}{\sigma S}I_{i\phi}\right)$$

As such, $I_{j\phi}$ cannot be obtained because the equation is a mixture of $I_{j\phi}$ and $I_{i\phi}$. However, the resistance matrix of the attenuation term shown below is diagonal and has only the elements of $i = j$, so it can be unified to $I_{j\phi}$.

$$\Lambda I_{j\phi} = -M_{ij}^{-1}\frac{dM_{ij}}{dt}I_{j\phi} - M_{ij}^{-1}u_{ir}\frac{1}{r_i}M_{ij}I_{j\phi} - M_{ij}^{-1}R_{ij}I_{j\phi} \tag{13}$$

Here, Λ indicates the eigenvalues. (13) is obtained. These simultaneous equations are used here to obtain the Λ values. R_{ij} is a matrix of the resistance and a function of the coil circumference and cross-sectional area S, where S is calculated from the thickness T and the section of the flow course as $S = (2\pi R_0 T)/16$. Then, $R_{ij} = 2\pi r_i/(\sigma S) = (16 r_i)/(\sigma R_0 T)$. R_{ij} is a diagonal matrix because the voltage drop exists only for $i = j$.

2.2.2 Method for Calculating the Inductance

The inductance used in the example calculation (see Figs. 3(a) and (b)) is as follows. In the coil description (Fig. 2), the coil's cross-sectional area and shape are disregarded to calculate the inductance because these geometrical factors introduce a large degree of complexity. Therefore, the coil is treated in the calculation, and Fig. 3 is approximated as a thin line. $\boldsymbol{A}_j$[12] is calculated as follows:

$$\boldsymbol{A}_j = \frac{\mu}{4\pi}\oint_{C_j}\frac{\boldsymbol{J}_j}{l}dV = \frac{\mu}{4\pi}\oint_{C_j}\frac{\boldsymbol{J}_j S}{l}ds_j = \frac{\mu}{4\pi}\oint_{C_j}\frac{\boldsymbol{I}_j}{l}\cos\phi ds_j = \frac{\mu}{4\pi}\boldsymbol{I}_j\oint_{C_j}\frac{\cos\phi}{l}ds_j, \tag{14}$$

where l is the distance between ds_i and ds_j, μ is the magnetic permeability, dV is the infinitesimal volume, and S is the cross-sectional area of the current (i.e., the coil). When only ϕ directional components are handled, $I_{j\phi} = J_{j\phi}S$ is the current, and the directional element for ds_i of $I_{j\phi}$ is $I_{j\phi}cos\phi$. By substituting (7) for $A_{j\phi}$ in (14), (15) is obtained as follows:

$$M_{ij} = \frac{2\pi r_i}{I_{j\phi}} \frac{\mu}{4\pi} I_{j\phi} \oint_{C_j} \frac{\cos\phi}{l} ds_j = 2\pi r_i \frac{\mu}{4\pi} \oint_{C_j} \frac{\cos\phi}{l} ds_j \tag{15}$$

When μ is set to $4\pi \times 10^{-7}$H/m (vacuum conditions), (16) is obtained as follows:

$$M_{ij} = 2\pi r_i \oint_{C_j} \frac{\cos\phi}{l} ds_j \times 10^{-7} \tag{16}$$

M_{ij} is calculated by summing (17), where C_j is divided into $k = 100$ equal parts, $\Delta s_j = \frac{2\pi r_j}{100}$, as follows:

$$M_{ij} \approx 2\pi r_i \sum_{k=1}^{100} \frac{\cos\phi_k \Delta s_j}{l_k} \times 10^{-7} \tag{17}$$

$$l_k = \sqrt{(r_j \cos\phi_k - r_i)^2 + (r_j \sin\phi_k)^2 + (z_j - z_i)^2} \tag{18}$$

The angle of a specific coil n is given by $\theta_n = 2\pi n/16$, where $r_n = r_0 + R_0 \cos\theta_n$ and $z_n = R_0 \sin\theta_n$ (Fig. 2). Previously, i and j were used in mutual inductance calculations to distinguish between the coils that received electromotive force and the coils that had a current flow. Each number n is replaced by i or j for any two of the coils.

2.2.3 Power Generation Trends

The nature of this power generation is described in terms of the equation obtained above.

(13) and (15) are used to explain the tendency of the inductance to change because of convection. The variable r_i is included in (15), and z_i is contained in l_k (18). Thus, power generation is related to the velocity of convection in the Ra and Z directions. That is, $\frac{dM_{ij}}{dt}$ is driven by poloidal convection. In this drive, not only the change in self-inductance but also the change in mutual inductance is important because the mutual coupling tends to fluctuate because of the difference in convection when the coils are far apart.

When r_0, R_0 and T in Fig. 2 change in a similar form, r_i, r_j, z_i and z_j in (17) and (18) change in a similar form so that the components of M_{ij} are similar to each other, and the value changes proportionally. In other words, the results of this numerical calculation can be predicted to change similarly when the scale of the system is changed.

Predicting from $\frac{dM_{ij}}{dt}$ on the first right-hand side of (13), when M_{ij} decreases, this term becomes positive, and power generation may occur against the attenuation term of the third term. Therefore, if power generation occurs, the place is the second quadrant (top left of P_c in Fig. 2). In brief, the inductance generally increases with the radius of the coil, and conversely, the smaller the radius is, the smaller the inductance.

In the second quadrant, the inductance decreases because the radius of the coil is decreasing due to convection, so the change is of negative polarity. This phenomenon is explained in Appendix A by the nature of numerical calculation formulas using (17) and (18).

2.2.4 Elements of other Expressions

$\frac{dM_{ij}}{dt}$ is calculated as the difference in M_{ij} induced by the flow velocity over an infinitesimal divided by $\Delta t(ex.1.0 \times 10^{-6}s)$.

The velocity $\boldsymbol{U}$ depends on the θ_n of each coil and is calculated as follows (Fig. 2):

$$|\boldsymbol{U}| = \frac{r_0}{r_i}\omega R_0,\ u_r = -|\boldsymbol{U}|\sin\theta_n,\ u_z = |\boldsymbol{U}|\cos\theta_n. \tag{19}$$

where ω is the angular velocity of the flow. The properties of cylindrical coordinates appear in (13) as electromagnetism and in (19) as convection. In other words, convection is set in cylindrical coordinates where a torus-like fluid flows in the poloidal direction. $\frac{1}{r_i}$ is multiplied because a fluid of the same volume is concentrated and dispersed towards the Z axis in a poloidal flow such that the flow path expands and contracts, and the velocity changes accordingly. $\frac{r_0}{r_i}$ is a coefficient that adjusts on the basis of the position of r_0 so that the flow rate satisfies the continuity equation.

Furthermore, M_{ij}^{-1} is the inverse matrix of M_{ij}.

3 Calculation Conditions and Results

3.1 Calculation conditions

The conditions for the numerical calculations are as follows.

The general conditions are $R_0 = 1000$ m, $r_0 = 2000$ m, and $T = 0.1R_0$. The electrical conductivity σ is 10^3 s/m (solar convection zone)[9]. The velocity of convection is given by (19), where $|\boldsymbol{U}| = \frac{r_0}{r_i}\omega R_0$. As a condition, the angular velocity ω is set to $2\pi 2.1 \times 10^{-3}$, where only the maximum eigenvalue is barely positive. In other words, we set the conditions that seem to be the boundary at which power generation begins to occur.

3.2 Results

The result calculated on the basis of (13) is shown under the conditions above. The eigenvalues $\Lambda(\lambda_1 - \lambda_{16})$ are listed in Table 1. A positive value is highlighted in bold in the table. Only the maximum eigenvalue, λ_{16}, has positive polarity. Although it has positive polarity, the absolute value is small. This result is obtained because the calculation conditions were set in a specific way. Thus, under these conditions, power generation begins. In addition, if the convection speed is high, the power generation will be strong. The eigenvector of the maximum eigenvalue is shown in Table 2. The length of each component of this eigenvector is adjusted so that the norm is 1. This condition indicates that the absolute value of the current is maximised in Coil 6, which is highlighted in bold. These components indicate the current values of each coil.

Table 1 Eigenvalues Λ. The eigenvalue is calculated numerically. Assuming the boundary of the start of magnetic field generation, the calculation condition was set to generate one eigenvalue that was barely positive. Therefore, only $\lambda 16$ is positive.

Λ	Eigenvalue
λ_1	-5.290×10^{-1}
λ_2	-3.221×10^{-1}
λ_3	-2.288×10^{-1}
λ_4	-1.762×10^{-1}
λ_5	-1.431×10^{-1}
λ_6	-1.208×10^{-1}
λ_7	-1.084×10^{-1}
λ_8	-9.134×10^{-2}
λ_9	-8.964×10^{-2}
λ_{10}	-6.714×10^{-2}
λ_{11}	-6.575×10^{-2}
λ_{12}	-5.037×10^{-2}
λ_{13}	-4.163×10^{-2}
λ_{14}	-2.918×10^{-2}
λ_{15}	-1.633×10^{-2}
λ_{16}	$\mathbf{7.729 \times 10^{-3}}$

This table is used to create the following figure. The lattice-like distribution of the magnetic field generated from the current state (based on the eigenvector) is shown in Fig. 5. It is vectorially displayed on the Z-Ra plane. These lengths are compressed by square roots. The square root was set so that the length of the line of the magnetic field display was not extremely different. The circle centred on P_c indicates the convection path. Each small round mark on the convection circle indicates the location of the coil (Fig. 2(b)). The range of the figure is $\pm 2R_0$ in the Z direction and $+4R_0$ in the Ra direction. The lattice spacing is $\frac{R_0}{5}$ for Z and Ra. Since the magnetic field is not a specific value that has increased, its unit is not displayed. Note that some vectors near small round marks on convection are unnatural in size and direction. This result was obtained because the lattice points for calculating the magnetic field distribution and the position of the coil were too close together, so the extreme values were calculated.

The calculation method of the magnetic field is as follows. The calculation of the inductance is obtained through the calculation of the vector potential, as shown in (14). Therefore, the vector potential was calculated using the inductance calculation method. That is, via (7), the vector potential was obtained through the current of the coil and the temporary inductance at each location. Furthermore, the value related to the rotation of the vector potential at each location was obtained and converted to a magnetic field via (2).

Table 2 Eigenvector of the maximum eigenvalue in Table 1. This eigenvector corresponds to the current distribution flowing through each coil. The combined current is adjusted to 1. The current is maximised at Coil 6.

Coil number	Eigenvector
0	2.262×10^{-2}
1	4.870×10^{-2}
2	9.259×10^{-2}
3	1.691×10^{-1}
4	2.979×10^{-1}
5	4.806×10^{-1}
6	$\mathbf{6.198 \times 10^{-1}}$
7	4.801×10^{-1}
8	1.193×10^{-1}
9	-5.597×10^{-2}
10	-6.638×10^{-2}
11	-4.792×10^{-2}
12	-3.188×10^{-2}
13	-1.899×10^{-2}
14	-7.231×10^{-3}
15	5.626×10^{-3}

In Fig. 6, the intensity of the magnetic force is represented by contour lines to elucidate the magnetic force distribution of Fig. 5. On a poloidal surface, it is a line, but in three-dimensional space, it is a curved surface whose line is rotated on the axis of symmetry. Since it is a cylindrical coordinate, the magnetic force, that is, the magnetic flux density, even if the same number of magnetic fluxes passes, the cross-sectional area of the passage changes according to the distance r from the axis of rotational symmetry Z, so the magnetic flux density changes. Therefore, in the contour line, the magnetic force is corrected by multiplying the circumference by $2\pi r$.

In Fig. 6 , the yellow pointillism line is the highest magnetic field level (warmer colours have a higher level). The circle in the figure is the hypothetical convection position shown in Fig. 2. Since there are yellow areas around the second quadrant (top left of P_c) of this circle, it is thought that power generation mainly occurs there. In this study, convection is examined only at the position of 16 coils on the convective circle shown in Fig. 2, so it is difficult to understand because the contour lines of the same level are divided into multiple parts and are intricate near the convection. In reality, the coils should be innumerably distributed so that the contour lines are continuous and smooth. If we increase the number of coils and place them inside the torus convection system, we will probably be able to draw smoother and more accurate contour lines near the convection system.

Figs. 5 and 6 are rotationally symmetric around the Z-axis, and numerical calculations show that an axisymmetric magnetic field arises from axisymmetric poloidal convection on the same axis.

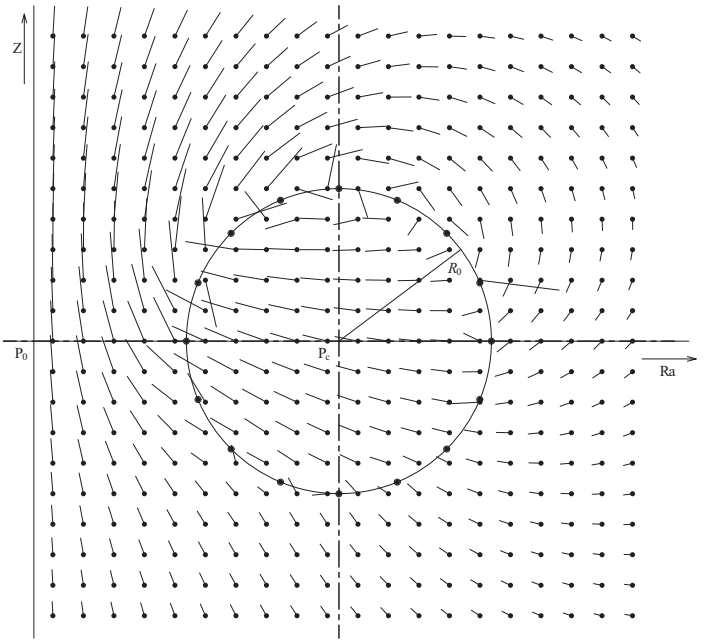

Fig. 5 Magnetic field distribution generated from the current state on the basis of the results of numerical calculations. This magnetic field distribution is vectorially drawn on the Z-Ra plane on the basis of eigenvectors (Table 2). These lengths are compressed by square roots. The range of the figure is $\pm 2R_0$ in the Z direction and $+4R_0$ in the Ra direction. The lattice spacing is $\frac{R_0}{5}$ for Z and Ra. Since the magnetic field is not a specific value that has increased, its unit is not displayed.

3.3 Similarity of Scale

Table 3 shows the trend of power generation on the convection scale. The trend mentioned in Section 2.2.3 Power Generation Trends also appeared in the calculations. From left to right in this table, the scale R_0 of the convection system, the angular velocity ω of the convection system, the positive maximum eigenvalue λ_{max}, and the positive maximum eigenvalue λ_{max}N when the second term on the right-hand side of (13) is nonfunctioned. This table shows that increasing the scale of convection by 3 orders of magnitude decreases the convection velocity by 6 orders of magnitude, resulting in a similar positive eigenvalue that is 6 orders of magnitude smaller. In other words, it becomes easier to generate electricity by squaring the convective scale. λ_{max}N is described in Section 4.3, Resistance Losses in Stationary Fluids Around Set Convection.

As estimated under other conditions, as long as the numerical values of R_0, r_0, and T change in a similar form, the eigenvalues also change in a similar form if the flow velocity is appropriate. In other words, since the interval ratio or polarity of the eigenvalues does not change, the nature of magnetic field generation is the same even if the scale of convection changes.

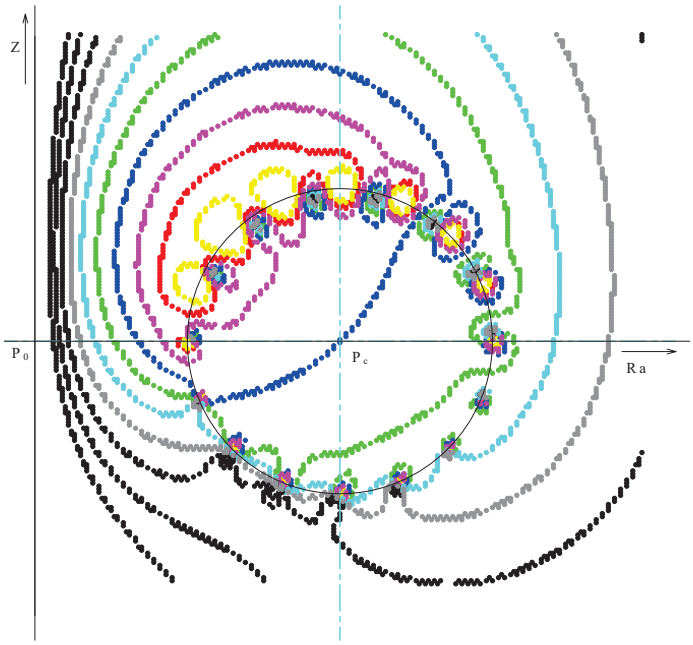

Fig. 6 Magnetic force contour lines generated from the current state on the basis of the results of the numerical calculations. This figure shows the magnetic force contour lines drawn on the Z-Ra plane on the basis of eigenvectors (Table 2). The range of the figure is $\pm 2R_0$ in the Z direction and $+4R_0$ in the Ra direction. Since the magnetic field is not a specific value that has increased, its unit is not displayed. Ten contour lines are displayed. A strong magnetic field is displayed in a warm colour.

Table 3 Maximum eigenvalues according to the size of the convective system and maximum eigenvalues without the second term on the right-hand side of (13) at the angular velocity of convection at which power generation starts.

R_0 km	ω rad/s	λ_{max}	$\lambda_{max}N$
1	$2\pi 2.1 \times 10^{-03}$	7.729×10^{-03}	3.578×10^{-04}
1000	$2\pi 2.1 \times 10^{-09}$	7.729×10^{-09}	3.578×10^{-10}

4 Discussion

As described above, the underlying electromagnetic induction equation was derived, and the result was obtained via numerical calculation as a system eigenvalue problem. The results revealed the start of power generation by generating an axisymmetric magnetic field from poloidal convection. Here, the results and problems of this numerical calculation are discussed in detail below.

4.1 Generation of Axisymmetric Magnetic Fields

A positive eigenvalue means that the eigenvector increases exponentially as a function of the eigenvalue. The eigenvector of the maximum eigenvalue of positive polarity is shown in Table 2. Each component indicates the current in each coil. However, this

eigenvalue or eigenvector only means that power generation starts, and the state starts at the beginning. Therefore, the magnetic field in the figure is initially considered weak. However, the electric current increases over time. The larger the eigenvector is, the faster the magnetic field grows. When self-excited power generation occurs and the magnetic field increases, the magnetic field becomes more pronounced, as shown in Figs. 5 and 6. The following discussion can be drawn from this figure.

A strong magnetic field originates around the second quadrant of convection and passes through the convection circle. In other words, a strong magnetic field intersects with convection and seems to contribute to power generation. In addition, outside the strong magnetic field, a weak magnetic field passes near the Z-axis and circulates on the outside away from convection. Since this surface is rotationally symmetric around the Z axis, it shows a rotationally symmetrical magnetic force in the poloidal flow.

Notably, the magnetic field in these figures is asymmetric at $\pm$Z of the line-symmetry line (the line in the Ra direction on P_0-P_c). This asymmetry arises mainly because the position where power generation is likely to occur is at +Z.

4.2 Possibility of Magnetic Field Stabilisation

The self-excited power generation discussed above becomes more powerful because the magnetic field increases when power generation starts. Once the magnetic field strengthens, even if convection weakens from the start, power generation continues. This process continues even if the power generation consumes the energy of convection, and the convection speed decreases. If the convection velocity decreases further, the intensity of power generation will naturally weaken. Eventually, a balance will emerge somewhere, depending on the ability to supply convective energy from the external environment. In other words, it might be stabilised at the strength of a certain magnetic field. The behaviour of convection and the energy supply capacity of convection must be examined to determine whether it is actually stable, but this undertaking is not the subject of this paper.

Another assumption is that the magnetic field may be stabilised. When the current increases to a certain extent, the Lorentz force acts. This force acts in the opposite direction of convection, thus reducing the flow velocity. This behaviour will suppress power generation, so a possibility exists that a balance between power generation and a decrease in flow velocity will occur at some level. In other words, the magnetic field may be stabilised. Again, it is necessary to examine how convection behaves with respect to the Lorentz force, which is beyond the scope of this paper.

4.3 Resistance Losses in Stationary Fluids around Set Convections

Since this calculation ignores the resistance loss in the surrounding fluid that is not convection, the generation of electricity is considered easier. Electromagnetic induction also generates an electric current in the surrounding fluid, which causes resistance loss. However, this electromagnetic induction occurs when the current changes. This resistance loss occurs because the current changes. It is a loss caused by an increase in current. Loss occurs because of electromagnetic induction due to an increase in current,

and the eigenvalue is suppressed. However, this does not mean that the current does not increase. That is, the maximum positive eigenvalue is less than that in Table 1 instead of being negative.

Furthermore, the second term on the right-hand side of (13) plays an important role. According to the estimation, the eigenvalue λ_{max} when this term is included, as shown in Table 3, is more than one order of magnitude larger than λ_{max}N when it is omitted. This result is obtained because once power generation starts, the term works more strongly because of the generated current, and power generation becomes more powerful. Since this potent power generation is thought to strongly overcome the loss of nonconvection fluids, the positive eigenvalue is not considered so small even if the loss due to the surrounding stationary fluid is included. If the current is subsequently stabilised by Section 4.2, electromagnetic induction does not occur in the surrounding fluid; thus, the loss of stationary fluid does not occur.

4.4 The Problem of Coils with Currents being Carried Away by Convection

Thus far, we have used numerical calculations to investigate the possibility of magnetic field growth, but there is a question here. Coils are moving with convection. Then, because the magnetic field freezes [13], convection and the magnetic field move together. In other words, the electric current results from power generation, and its associated magnetic field moves with convection. Since the current is carried with the movement of the coil, continuous growth of the magnetic field at a given location cannot be expected. Even if a coil reaches the highest point of power generation, it will pass by immediately. In this case, the little time for the magnetic field to grow continuously is a concern. To continuously generate power at the apex, even if the fluid, that is, the coil, moves with convection, the current and the associated magnetic field should not move.

However, in this work, we assume that the magnetic field grows in a specific location. The basis is the inductance considered in this paper. (13) is used for the numerical calculations and includes the mutual inductance. If we consider the change in time here, that is, the change in the current and the resulting change in magnetic flux, then Lenz's law[12] can be considered.

Here, we explain the meaning of the phrase "combination of mutual inductance and Lenz's law", which we use as the key point of this paper. The inductance is related to the relationship between the magnetic field and current ($\Phi_1 = L_1 I_1 + M_{12} I_2 + M_{13} I_3 + \ldots$). Lenz's law refers to the effect of generating an electromotive force E in the direction of suppressing the change in the magnetic field in a circuit ($E = -\frac{d\Phi}{dt}$). When combined, these results indicate that an electromotive force that suppresses the change in current is generated, including other circuits ($E_1 = -L_1 \frac{dI_1}{dt} - M_{12} \frac{dI_2}{dt} - M_{13} \frac{dI_3}{dt} \ldots$). This process is called "mutual induction". This electromotive force causes a current in the circuit in the direction of suppressing the change in the current of these circuits. In this paper, the action of the mutual inductance part is used as the basis for the discussion.

For example, if the current increases in the coil at one position, a current in the opposite direction is generated in the coil at the other position. Conversely, if the

current decreases in the coil at one position, a current in the same direction is generated in the coil at the other position. At the position where the current is at its peak, the coil exiting and the coil entering that position are adjacent to each other, so the current of the incoming coil increases as the current of the outgoing coil decreases. That is, at that position, the current is inherited by the next coil. This new concept has not been introduced in other theories. Hereinafter, this effect is abbreviated as the inheritance effect.

Therefore, current growth (magnetic field growth) at a specific position is considered possible. The matrix on the right side of (13) for calculating the eigenvalues in this paper includes the mutual inductance (other than M_{ii}.) This matrix is subsequently solved as an eigenvalue problem to obtain the change (eigenvalues) in the current (eigenvectors). Therefore, this eigenvalue can be expected to have the property of not moving at a specific position. In other words, the magnetic field continues to grow at a specific position according to the calculated eigenvalue. Furthermore, in real convection, since countless coils are close to each other, the coupling of mutual inductance is considered strong. Therefore, the inheritance effect is considered to work efficiently. In summary, even if the magnetic field is frozen, the calculated eigenvalues and eigenvectors do not move with the movement of each coil but represent the behaviour of the current remaining at the coil set position (Fig. 2).

4.5 Magnetic Diffusivity

In this work, magnetic diffusivity is ignored. The magnetic field should be attenuated depending on the magnetic diffusivity. However, the attenuation term of (13) contains a component corresponding to a magnetic diffusivity of $\frac{1}{\mu\sigma}$ (M_{ij}^{-1} contains $\frac{1}{\mu}$). Therefore, the magnetic diffusivity is already considered in the numerical calculation results. However, in this case, the current of the coil is considered in the calculation. The calculation results do not indicate what happens to the magnetic field generated outside the coil. We have not yet determined how much magnetic diffusivity works.

4.6 Relationship with Cowling's Theorem

The results of the calculations in this paper contradict Cowling's theorem. In this work, we assume that this calculation is correct, but it is a future task to elucidate the cause of this discrepancy.

4.7 The End of Discussion

Therefore, it has been shown that an axisymmetric poloidal magnetic field grows because of axisymmetric convection. In addition, the magnetic field stability can be maintained depending on the conditions.

Here, we present an imaginary diagram of our assumption about how this magnetic field occurs in celestial bodies. Suppose that a downdraft occurs in a conductive fluid at the poles of a celestial body. Assuming that a poloidal flow is generated in a torus-shaped fluid in this way, Fig. 7 depicts a virtual magnetic field with reference to Figs. 5 and 6. If a magnetic field is generated at the opposite pole in the same way, the connected magnetic field spreads over a wide area outside the celestial body.

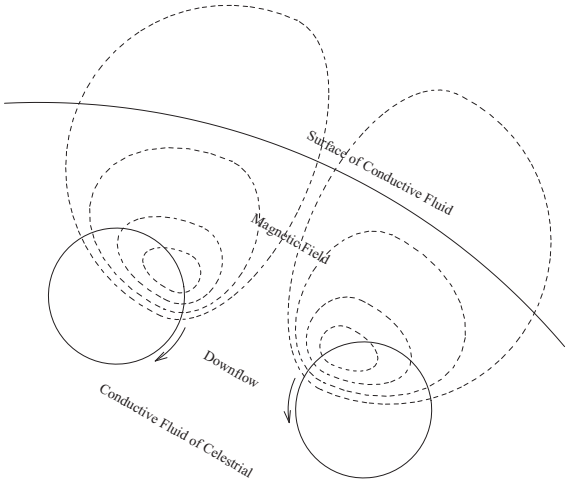

Fig. 7 An example of poloidal axisymmetric convection and a magnetic field in a celestial body. The solid arrows indicate fluid flow, whereas the dashed lines indicate the induced magnetic field. This figure is schematically drawn on the basis of Fig. 6.

5 Conclusion

This paper argues that an axisymmetric magnetic field grows with purely simple convection. Unlike previous theories, our work suggests that an axisymmetric magnetic field can be grown from axisymmetric poloidal convection without complex convection. We believe that this proposal is novel, but some issues are unresolved. However, if this proposal is correct, then there is something to look forward to, as described below.

For example, as mentioned in Section 3.3 Similarity of Scale, if the size of the system changes, the eigenvalues will change in the same way if the flow velocity is appropriate. We believe that arbitrary convection can be created to some extent in an artificial plasma experimental facility (ex., magnetic mirror type) rather than in the natural world, so the results of this research may be useful when aiming to strengthen a magnetic field. However, since higher speed and turbulence-free convection are indispensable, a certain amount of technological innovation is required to achieve this goal. We believe that this goal will eventually be achieved. Thus, this paper is in the field of so-called magnetohydrodynamics, and we expect that it will be useful not only for astronomical bodies but also for research in plasma furnaces and sodium experimental facilities.

Declarations

Conflicts of interest

The author has no conflicts of interest to declare.

Funding

No funding was obtained for this work.

Data availability statement

The data described in the manuscript are available. No other data are available.

Appendix A Tendency of Inductance Changes due to Convection

(17), (18) and (19)are redescribed here:

$$M_{ij} \approx 2\pi r_i \sum_{k=1}^{100} \frac{\cos\phi_k \Delta s_j}{l_k} \times 10^{-7}, \Delta s_j = \frac{2\pi r_j}{100} \tag{A1}$$

$$l_k = \sqrt{(r_j \cos\phi_k - r_i)^2 + (r_j \sin\phi_k)^2 + (z_j - z_i)^2} \tag{A2}$$

$$|\boldsymbol{U}| = \frac{r_0}{r_i}\omega R_0, \ u_r = -|\boldsymbol{U}|\sin\theta_n, \ u_z = |\boldsymbol{U}|\cos\theta_n. \tag{A3}$$

If the coil numbers i and j are set arbitrarily, the examination will be complicated, so the following procedure is performed. The large $\frac{dM_{ij}}{dt}$ of (13) greatly affects power generation. $\frac{dM_{ij}}{dt}$ is greatest when the convection velocity is high and the two coils are adjacent to each other. Therefore, the case where the two coils are in the same quadrant with a high flow velocity is considered. That is, consider the cases that are in the second and third quadrants. First, to make it easier to examine, the variable elements of M_{ji} are concentrated in a part of l_k in (A2). (A2) is transformed to $l_k = r_i r_j l'_k$. This $r_i r_i$ offsets the $r_i r_j$ of (A1). In this way, the elements of change can be concentrated on the remaining l'_k as follows:

$$l'_k = \sqrt{\left(\frac{1}{r_i}\cos\phi_k - \frac{1}{r_j}\right)^2 + \left(\frac{1}{r_i}\sin\phi_k\right)^2 + \left(\frac{z_j - z_i}{r_i r_j}\right)^2} \tag{A4}$$

Since the flow velocity is multiplied by $\frac{1}{r_i}$, as shown in (A3), in the second quadrant, as shown in Fig. 2, as the angle θ increases, r_i decreases, so the flow velocity increases. Then, the difference between z_i and z_j increases because u_z increases. Moreover, since the velocity u_z of (A3) also increases with θ, a further difference between z_i and z_j emerges. Therefore, $z_j - z_i$ of (A4) becomes larger. Simultaneously, the mutual inductance of (A1) decreases, so the time change has a negative polarity.

Note that (A4) has variable elements $\frac{1}{r_i}$, $\frac{1}{r_j}$ and $\frac{1}{r_i r_j}$. In the second quadrant, $\sin\theta$ decreases as the angle θ increases, so r_i, r_j and $r_i r_j$ decrease. Since each term in the square root of (A4) increases, l'_k increases. Since the inductance of (A1) decreases, the time change in inductance is negative in the second quadrant.

In the third quadrant, the opposite is true, and the change in mutual inductance tends towards positive polarity.

In summary, the change in inductance tends to be negative in the second quadrant and positive in the third quadrant.

References

[1] Levy, E.H.: Generation of planetary magnetic fields. Annu. Rev. Earth Planet. Sci. **4**, 159–185 (1976)

[2] Parker, E.N.: Hydromagnetic dynamo models. Astrophysical J. **122**, 293–314 (1955)

[3] Cowling, T.G.: The magnetic field of sunspots. Monthly Notices Roy. Astronomical Soc. **94(1)**, 39–48 (1933)

[4] Masada, Y., Sano, T.: Mean-field modeling of an $\alpha 2$ dynamo coupled with direct numerical simulations of rigidly rotating convection. The Astrophysical Journal Letters **794(1)**, 6 (2014)

[5] Sheremetyeva, Olga V., Godomskaya, Anna N.: The modes of magnetic field generation in a low-mode model of $\alpha\omega$-dynamo with α-generator varying intensity regulated by a function with an alternating kernel. EPJ Web Conf. **254**, 02015 (2021) https://doi.org/10.1051/epjconf/202125402015

[6] M. STEENBECK, F.K., RÄDLER, K.-H.: Berechnung der mittleren lorentzfeldstärke $\overline{b \times B}$ für ein elektrisch leitendes medium in turbulenter, durch coriolis-kräfte beeinflußter bewegung. Institut für Magnetohydrodynamik Jena der Deutschen Akademie der Wissenschaften zu Berlin **21 a**, 369–376 (1966)

[7] J. J. Love, D.G.: Dynamos driven by poloidal flow exist. Geophys. Res. Lett. **23(8)**, 857–860 (1996)

[8] Matthews, P.C.: Dynamo action in simple convective flows. Mathematical, Physical and Engineering Sciences **455**, 1829–1840 (1985)

[9] Cardin, P., Cugliandolo, L.G.: Dynamos: Lecture Notes of the Les Houches Summer School 2007. Les Houches, vol. 88, p. 496. Elsevier Science, Oxford (2011). https://books.google.co.jp/books?id=OVgaews3C1IC

[10] Otsuki, M.: Boosting the Magnetic Field of a Toroidal Conductive Fluid by a Poloidal Flow. Preprint at https://doi.org/10.51094/jxiv.284 (2023)

[11] Moffatt, K., Dormy, E.: Self-Exciting Fluid Dynamos. Cambridge Texts in Applied Mathematics. Cambridge University Press, Cambridge (2019)

[12] Rojansky, V.B., Rojansky, V.: Electromagnetic Fields and Waves. Dover Books on Physics Series. Dover Publications, New York (1979). https://books.google.co.jp/books?id=Zfk2E5pkwy0C

[13] Alfvén, H.: On the Existence of Electromagnetic-Hydrodynamic Waves. Arkiv for Matematik, Astronomi och Fysik **29B**, 1–7 (1943)

[14] Zeldovich, Y.B.: The magnetic field in the two-dimensional motion of a conducting turbulent fluid. Sov. Phys. JETP. **4**, 460–462 (1957)

[15] Bullard E.C., G.H.: Homogeneous dynamos and terrestrial magnetism. Phil. Trans. R. Soc. Lond. A **247**, 213–278 (1954)